Physics of Plasmas

Energy dissipation during magnetic reconnection in the Keda linear magnetized plasma device

Cite as: Phys. Plasmas **29**, 102108 (2022); https://doi.org/10.1063/5.0090790
Submitted: 09 March 2022 • Accepted: 21 September 2022 • Published Online: 27 October 2022

Longlong Sang, Quanming Lu, Jinlin Xie, et al.

Energy dissipation during magnetic reconnection in the Keda linear magnetized plasma device

Cite as: Phys. Plasmas **29**, 102108 (2022); doi: 10.1063/5.0090790
Submitted: 9 March 2022 · Accepted: 21 September 2022 ·
Published Online: 27 October 2022

View Online Export Citation CrossMark

Longlong Sang,[1,2] Quanming Lu,[1,2,a)] Jinlin Xie,[3,a)] Feibin Fan,[1,2] Qiaofeng Zhang,[1,2] Weixing Ding,[1,2] Jian Zheng,[3] and Xuan Sun[3]

AFFILIATIONS

[1]CAS Key Laboratory of Geospace Environment, School of Earth and Space Sciences, University of Science and Technology of China, Hefei 230026, China
[2]CAS Center for Excellence in Comparative Planetology, Hefei 230026, China
[3]CAS Key Laboratory of Geospace Environment, School of Nuclear Science and Technology, University of Science and Technology of China, Hefei 230026, China

[a)]Authors to whom correspondence should be addressed: qmlu@ustc.edu.cn and jlxie@ustc.edu.cn

ABSTRACT

This paper investigates energy dissipation during electron-scale magnetic reconnection with laboratory experiments. Magnetic fields with opposite directions are generated by two parallel identical pulsed currents in our Keda linear magnetized plasma device. Magnetic reconnection is realized in the rising phase of the pulsed currents. The ramp-up rate of the pulsed current is found to be proportional to the inflow speed, providing a method to modify the reconnection drive. The incoming magnetic energy and its dissipation into plasma energy have been estimated in the vicinity of the X line. It is found that the plasma energy converted from the incoming electromagnetic energy increases with the increasing reconnection drive, while the conversion ratio remains almost unchanged, which is about 10%.

I. INTRODUCTION

Magnetic reconnection is a fundamental physical process in plasma, where magnetic energy is dissipated into plasma energy including kinetic energy and thermal energy through the topological rearrangement of magnetic field lines. The energy source of explosive phenomena, such as solar flare and magnetospheric substorm in the space environment and the sawtooth in the laboratory fusion experiment, is considered to come from the magnetic field. Therefore, it is generally accepted that the underlying mechanism that governs these explosive phenomena is magnetic reconnection.[1–6]

The vicinity of the X line in magnetic reconnection is an important site at which magnetic energy is dissipated.[1,7] The reconnection electric field is induced in the vicinity of the X line when the magnetic field lines are brought by the inflow plasma toward the X line, broken in the vicinity of the X line, and then leave in the outflow region. The particles are energized by the reconnection electric field in the vicinity of the X line, and in this way, the magnetic energy is dissipated into plasma energy.[7] Both kinetic simulations and satellite observations have demonstrated that the reconnection electric field in the vicinity of the X line is balanced by the off diagonal electron pressure tensor term, and it can then work on charged particles and dissipate magnetic energy.[8–10] The reconnection rate is widely used to represent quantitatively the energy conversion from magnetic energy to plasma energy.[11] However, recent kinetic simulations have raised doubt that the reconnection rate can quantitatively describe energy dissipation in magnetic reconnection.[12] Therefore, energy dissipation in the vicinity of the X line is necessary to be confirmed in real physical process. A laboratory experiment can be reproducible and gives greater control of the plasma diagnosis compared to the single (or few) points passive measurement of satellite observation, providing a possible way to measure quantitatively energy dissipation during magnetic reconnection.[13]

Magnetic reconnection in the laboratory experiment has been realized in several well-designed laboratory plasma devices. One of the earliest reconnection experiments was conducted on a linear device at the University of California, Los Angeles, by Stenzel and Gekelman,[14,15] and other major experiments include the Todai Spheromak-3/4(TS-3/4),[16,17] magnetic reconnection experiments (MRX),[18,19] reconnection scaling experiments,[20,21] new terrestrial reconnection experiment (TREX),[22] CS-3D,[23] and VINETA II.[24,25] Yamada *et al.*[13] measured the conversion of magnetic energy to plasma energy during magnetic reconnection at the MRX facility and found that ~50% of magnetic energy was converted into plasma energy with about two-thirds going to ions and one-third going to electrons. Recently, Shi *et al.*[26] found that most of magnetic energy is converted into plasma energy in electron-scale reconnection with a strong guide field, which is different from traditional reconnection on an ion scale. This paper reports on magnetic reconnection experiments in an electron-scale current sheet with a finite guide field using our Keda linear magnetized plasma (KLMP) device. The dissipation of magnetic energy into plasma energy was measured at different drive currents.

The remainder of the paper is organized as follows. The experimental setup is introduced in Sec. II, and we describe the experimental results in Sec. III. The results of the study are summarized in Sec. IV.

II. EXPERIMENTAL SETUP

The magnetic reconnection experiments are performed in our KLMP device.[27] A diagram of the KLMP device is shown in Fig. 1(a). The vacuum chamber is 200 cm in length and 22.5 cm in diameter. Around the vacuum chamber, there are 12 sets of magnetic coils producing a steady axial magnetic field of 30 G, which confines the plasma and acts as a guide field in magnetic reconnection. The plasma source is a 15-cm-diameter oxide-coated cathode operating in the pulse mode with a frequency of 1 Hz and pulse length of 12 ms. A secondary anode is set at the end of the device, and a constant bias voltage is applied between the two anodes to make the plasma carry a background current. This will introduce additional electrons to overcome the axial current limit caused by the Bohm criterion,[24] which is beneficial to the occurrence of magnetic reconnection. The working gas is argon and the typical plasma parameters are given in Table I. The highly reproducible discharges provide the background plasma with electron density around $3 \times 10^{17}\ \mathrm{m^{-3}}$ and temperature about 3.6 eV. Because the electron collisional mean free path $\boldsymbol{\lambda_{mfp}} = V_{te}/\nu_{ei}$ (here, V_{te} is the electron thermal velocity, ν_{ei} is the electron–ion collision rate) is much larger than the scale of the characteristic length L (3 cm, the width of the current sheet) in our experiment, the collisionality parameter is $L/\lambda_{mfp} \ll 1$. In our experiments, reconnection is weakly collisional, and the plasma collisionality is not a dominant item during the energy dissipation.

The reconnection magnetic field is generated by two parallel 120-cm-long aluminum rods separated by 10 cm. Magnetic fields with opposite directions are induced when two identical pulsed currents I_p pass through the two aluminum rods. A programmable pulsed power source is used to provide the pulsed current, and the time evolution of the pulsed current is shown in Fig. 1(b). During the rising phase, the magnetic fields around the rods strengthen, and are pushed away from the rods toward the center of the chamber. In the experiments, we focus on magnetic reconnection in the rising phase of the pulsed current. The ramp-up rate of the currents can be modulated from 40 to 93 A/μs by changing the charging voltage of the power source. The characteristic length L is much smaller than the ion inertial length, which is about 10 electron inertial lengths. In addition, the ion gyroperiod is about 455–714 μs, which is much longer than the experimental time. All these points imply that the ions are unmagnetized and are not involved in magnetic reconnection directly. Only electrons are involved directly in magnetic reconnection, and magnetic reconnection in our KLMP experiments is electron-scale reconnection.

A probe array, which can move continuously in the x–z plane, is used to scan the reconnection section, and it comprises of two perpendicular magnetic coils and a Langmuir probe with four tips. The two magnetic coils are used to measure the magnetic field in the x and z

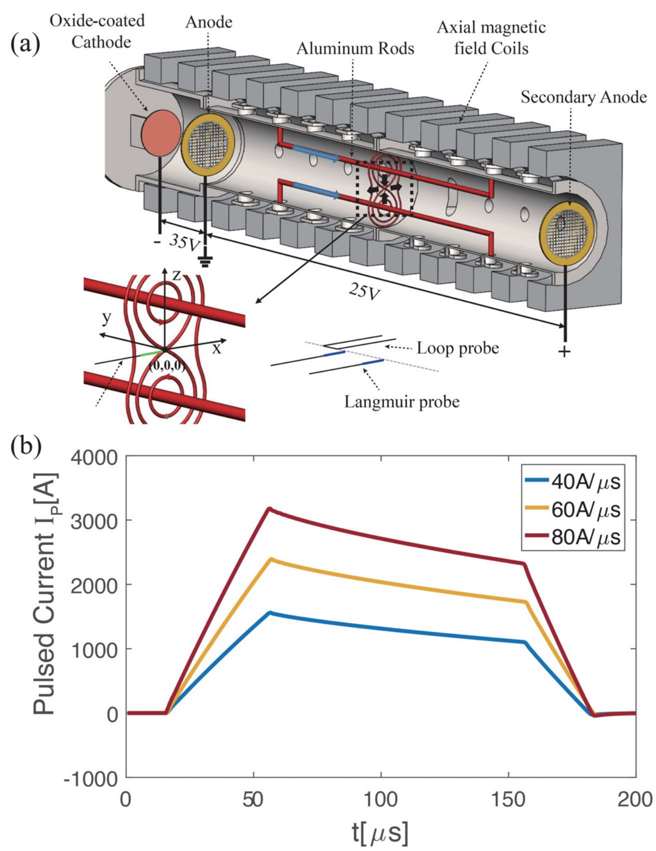

FIG. 1. (a) Schematic of the Keda linear magnetized plasma device and (b) time evolution of the pulsed currents in the rods with different ramp-up rates.

TABLE I. Typical argon plasma parameters of the KLMP device.

Parameter	Unit	Value
Plasma number density n	$\mathrm{m^{-3}}$	3×10^{17}
Electron temperature T_e	eV	3.6
Ion temperature T_i	eV	0.4
Reconnection magnetic field B_r	G	20–50
Background magnetic field B_g	G	30
Characteristic length L	cm	3
Electron inertial length d_e	mm	9.7
Ion inertial length d_i	m	2.63
Electron gyrofrequency f_{ce}	MHz	100–163
Ion gyrofrequency f_{ci}	kHz	1.4–2.2
Electron gyroradius r_e	mm	0.8
Ion gyroradius r_i	cm	8
Electron plasma frequency f_{pe}	GHz	4.91
Ion plasma frequency f_{pi}	MHz	18.2
Electron mean free path λ_{mfp}	cm	36
Electron–ion collision rate υ_{ei}	MHz	40

directions. A set of triple Langmuir probe is used to obtain the plasma potential and electron temperature in real-time, and a single Langmuir probe that measures ion saturation current is used to monitor plasma density. Here, the ion saturation current is employed to estimate the plasma density, ignoring the influence of the slight perturbation of electron temperature. The scanning ranges are x = [−5, 5 cm] and z = [−3, 3 cm], where the center of the chamber is set at (0, 0). Data are collected at 21 × 13 grid points that are spaced 0.5 cm apart in both the x and z directions. In this way, the distributions of the magnetic field and plasma density in the x–z section are obtained.

In Fig. 1(a), the axial (y-direction) electric field at the center of the chamber is measured by a set of probes including a loop probe and two separated triple Langmuir probe, which is similar to the probe system used by Stenzel *et al.*[28] Here, it is assumed that the reconnection electric field around the X line is almost uniform along the direction perpendicular to the reconnection plane, which has been proved in previous works of 3D numerical simulations[29] and relevant experiments with a guide field.[14,28] The loop probe comprises two radial wires and a short axial wire with a length $\Delta y = 3$ cm. Because the induced voltages on the two radial wires cancel each other out, the open-loop voltage of the probe V arises only from the induced voltage of the axial wire, and we get $V = E_{iy} \cdot \Delta y$, where E_{iy} is the induced electric field in the axial direction. In this way, the induced electric field can be determined using $E_{iy} = V/\Delta y$. Two separated triple Langmuir probes are set at different axial positions with spacing of $\Delta y = 20$ cm to measure the electrostatic field $E_{sy} = -\Delta\phi_P/\Delta y$, where ϕ_P is the plasma space potential. Here, it is assumed that the electrostatic field is uniform around the X line. The total axial electric field is then $E_y = E_{iy} + E_{sy}$. The induced axial electric field can be calculated using $E_{iy} = -\partial A_y/\partial t$, where A_y is the magnetic vector potential. Therefore, the induced electric field in the x–z plane can be derived using the measured induced electric field at the center and the magnetic field in the x–z plane. Moreover, a Rogowski coil measures the current in the *y* direction of the circular region with a diameter of 3.5 cm and center at (0, 0).

All the diagnostic data are collected using a National Instruments data acquisition card with a sampling frequency of 2 MHz.

III. EXPERIMENTAL RESULTS

We first present the experimental results for the intermediate pulsed currents with a ramp-up rate of 67 A/μs in Fig. 2. The results are shown for the plane in the middle of the vacuum chamber. In our experiments, magnetic reconnection can be considered as a 2D

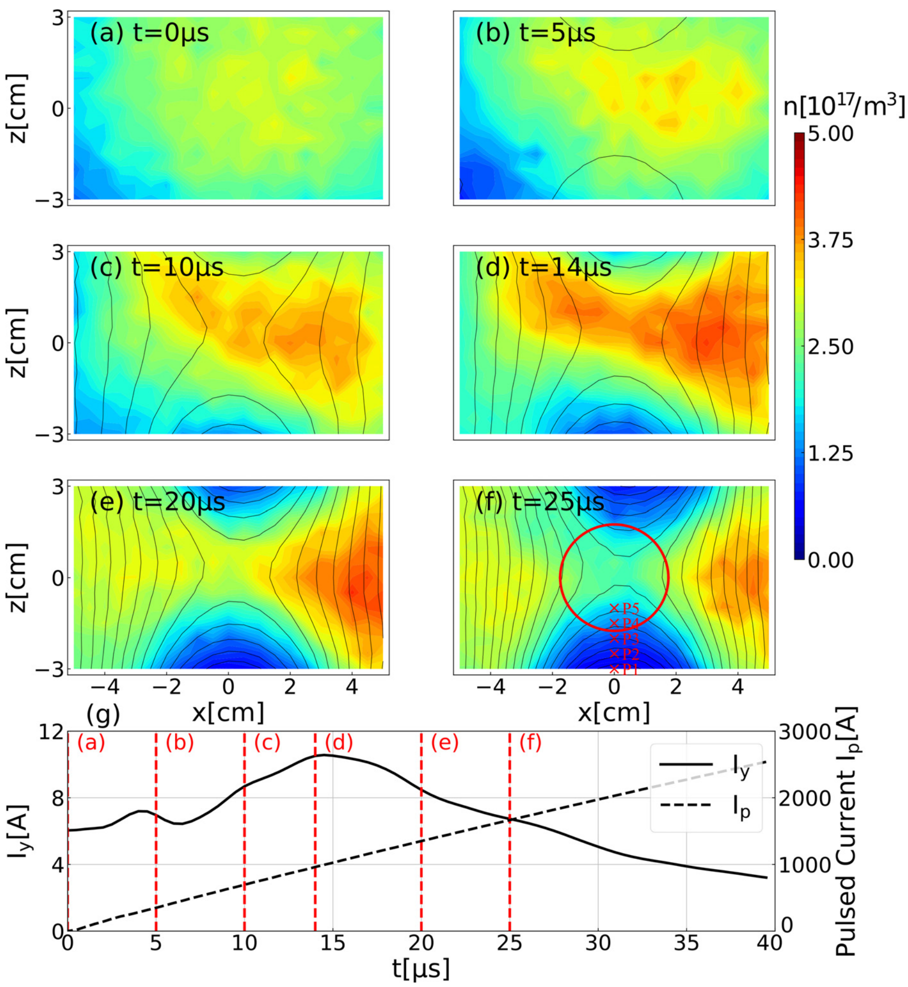

FIG. 2. Time evolution of the plasma density and magnetic field lines (black lines) in the x–z plane at (a) t = 0 μs, (b) t = 5 μs, (c) t = 10 μs, (d) t = 14 μs, (e) t = 20 μs, and (f) t = 25 μs at a ramp-up rate of 67 A/μs. (g) Out-of-plane current I_y at the center of the chamber measured by the Rogowski coil with a diameter of 3.5 cm (solid line) and the pulsed current in the rods I_P (black dashed line) for reference, and the times selected for (a)–(f) (red dashed lines).

process, and we can map the magnetic flied lines into the x–z plane. Using the measured x and z components of the magnetic field, we can calculate the y component of the vector potential at the point (x_1, z_1), which can be expressed as $A_y(x_1, z_1) - A_r(x_0, z_0) = \int_{x_0}^{x_1} B_z(x, z_0)dx - \int_{z_0}^{z_1} B_x(x_1, z)dz$. [Here, $A_r(x_0, z_0)$ is the magnetic vector potential at reference point (−5, 0 cm), and is recalibrated by the $A_y(0, 0)$ from the loop probe.] The magnetic field lines can then be represented by the contours of A_y. The pulsed current starts to rise at $t = 0$ μs. Figures 2(a)–2(f) show the time evolution of the magnetic topology and plasma density (n) at $t = 0$, 5, 10, 14, 20, and 25 μs, respectively. Figure 2(g) presents the time evolution of the pulsed current I_p in the aluminum rod and the current I_y measured by the Rogowski coil in a circular region. The amplitude of the generated magnetic field clearly increases with the pulsed current, and the magnetic field lines are squeezed into the center of the chamber. After $t = 5$ μs, an obvious X-type topology of magnetic field lines forms around (0, 0), and the plasma is compressed into the chamber center along with the moving magnetic field. Plasma density around (0, 0) increases with the rapid increasing of the out-of-plane current I_y measured by the Rogowski coil. Both the out-of-plane current and the plasma density around (0,0) reach their maximum values at approximately $t = 14$ μs. Due to the plasma ejection along the ±x outflow directions, the plasma around (0,0) is almost evacuated after 20 μs and the out-of-plane current also starts to decline, which results in a drastic change of the plasma background. Thus, we focus on the early phase of this "push" reconnection and leave the decline phase of the current I_y in the future investigation.

In order to explore the movement of plasma during the reconnection process, Fig. 3 shows the time evolution of the plasma density at five locations marked p1–p5 in Fig. 2(f), and a ramp-up rate of 53 A/μs is used. At the edge of experimental region, a plasma density peak caused by the compression appears at p1 first around 5 μs. Then, the density peak propagates toward the center along the z direction. We can estimate its propagation speed from the spatial location and the arrival time of the plasma density peak. Here, we think that the movement of electrons will cause an electrostatic field due to a strong charge separation, and then drag ions, which at last leads to the evolution of the plasma density.

In this way, the plasma velocities in the inflow region at different ramp-up rates of the pulsed currents are shown in Fig. 4. Here, the error bars of the inflow speed in Fig. 4 comes from the linear fitting of the points of the peak density in Fig. 3. Meanwhile, the drift speed in the inflow region is estimated by the reconnection electric field E_y and local magnetic field B_x. By varying the ramp-up rate of the pulsed current, the inflow velocity increases with the ramp-up rate and ranges from 3000 to 6000 m/s, and the results of those two calculation methods is highly consistent. This proves that the drive current can effectively modulate the inflow speed in our systematic experiment.

Assuming that physical parameters do not change along the y-direction, the energy dissipation during the reconnection process, which is the key to answering the question of how much magnetic energy is converted to plasma energy, can be described by

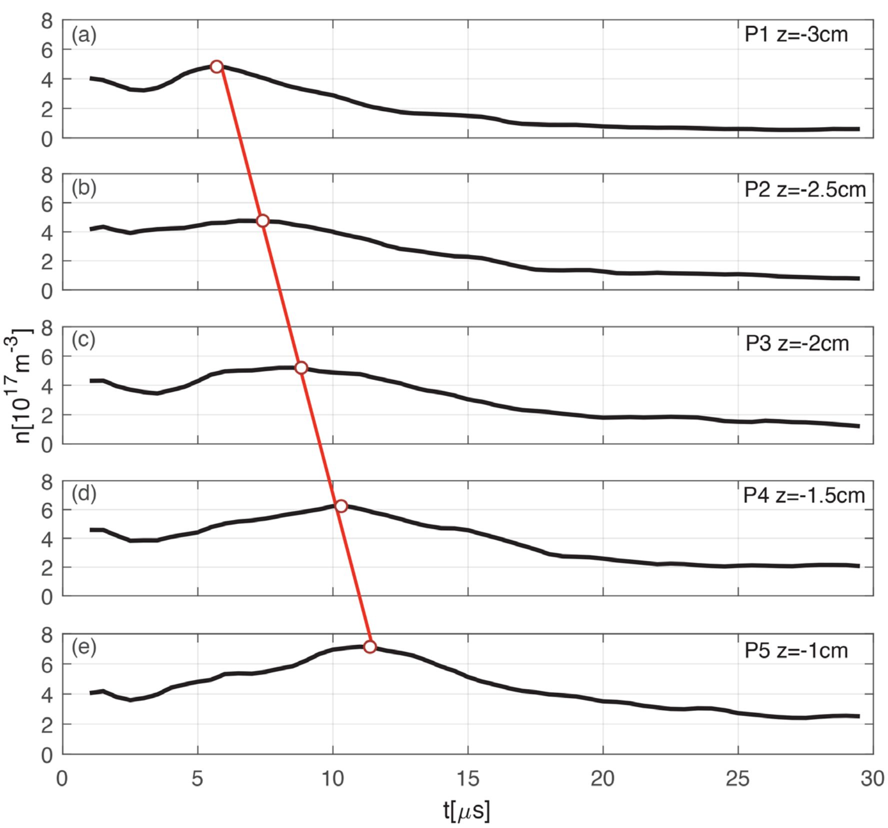

FIG. 3. (a)–(e) Time evolution of the plasma density at five locations spaced at intervals of 0.5 cm along the x = 0 axis from z = −3 to −1 cm at a ramp-up rate of 53 A/μs. The positions are labeled in Fig. 2(f).

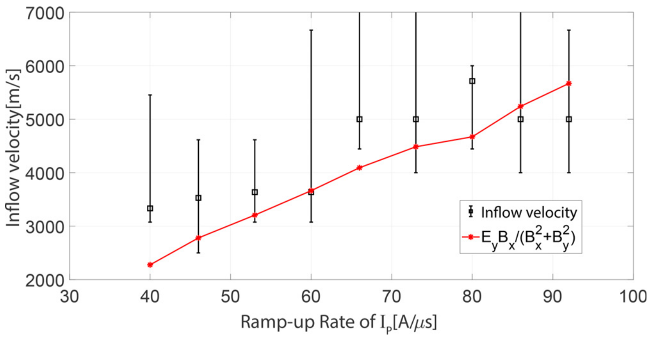

FIG. 4. Evolution of the measured inflow velocity and the drift speed in the inflow region estimated using the reconnection electric field E_y at different ramp-up rates of the pulsed current.

$$\int_S E\cdot J dS = \oint_l \left(\frac{1}{\mu_0}E\times B\right)\cdot dl - \frac{d}{dt}\int_S \frac{B^2}{2\mu_0}dS, \quad (1)$$

where S is a region in the reconnection plane encircled by the line l. The term on the left side is the power of the work done by the electric field on particles, or the energy that particles obtain per unit time. The first term on the right describes the electromagnetic energy that enters the region S per unit time, and the second term relates to the time evolution of the magnetic energy in the region S. Here, the electric field energy is neglected because it is several orders of magnitude smaller than the other terms ($\frac{\varepsilon_0 E^2}{2} \ll \frac{B^2}{2\mu_0}$). In our experiments, the region S is the square with sides 3 cm long centered at (0, 0) shown in Fig. 5(a).

We further assume that the out-of-plane current density is uniform in the region S and the measurement region of the Rogowski coil, and the out-of-plane current density J_y can be calculated using the current I_y. In addition, the in-plane current density is much lower than the out-of-plane current density and therefore negligible. We can get $\int_S E\cdot J dS \approx \int_S E_y J_y dS$. Moreover, the term $\oint_l(\frac{1}{\mu_0}E\times B)\cdot dl$ can be divided into $\oint_l(E_yB_x/\mu_0)\cdot dl - \oint_l(E_yB_z/\mu_0)\cdot dl$. The Poynting theorem then tells us that

$$\oint_S E_y J_y dS = \oint_l (E_yB_x/\mu_0)\cdot dl - \oint_l (E_yB_z/\mu_0)\cdot dl - \frac{d}{dt}\int_S \frac{B^2}{2\mu_0}dS, \quad (2)$$

where the power of the energy dissipation is $\oint_S E_y J_y dS$, the time evolution of the electromagnetic energy entering the region S per unit time from the inflow region is $W_{in} = \oint_l (E_yB_x/\mu_0)\cdot dl$, the electromagnetic energy leaving the region S per unit time to the outflow region is $W_{out} = \oint_l (E_yB_z/\mu_0)\cdot dl$, and the change of the magnetic energy in the denoted region is $W_B = \frac{d}{dt}\int_S \frac{\mathbf{B}^2}{2\mu_0}dS$. According to this deformation formula, all the elements in this equation become measureable physical quantities in our experiments.

Using the case at a ramp-up rate of 40 A/μs, Fig. 5(b) plots the time evolution of the dissipation of the electromagnetic energy $W_{dp} = W_{in} - W_{out} - W_B$. Most of the incoming electromagnetic energy from the inflow region flows to the outflow region, and the other is converted into magnetic energy and plasma energy. Comparing the left and right sides of the formula, two ways of calculating dissipated power is shown in Fig. 5(c); i.e., $W_{dp} = W_{in} - W_{out} - W_B$ and $W'_{dp} = \int_S E_y J_y dS$. Here, the error of the magnetic

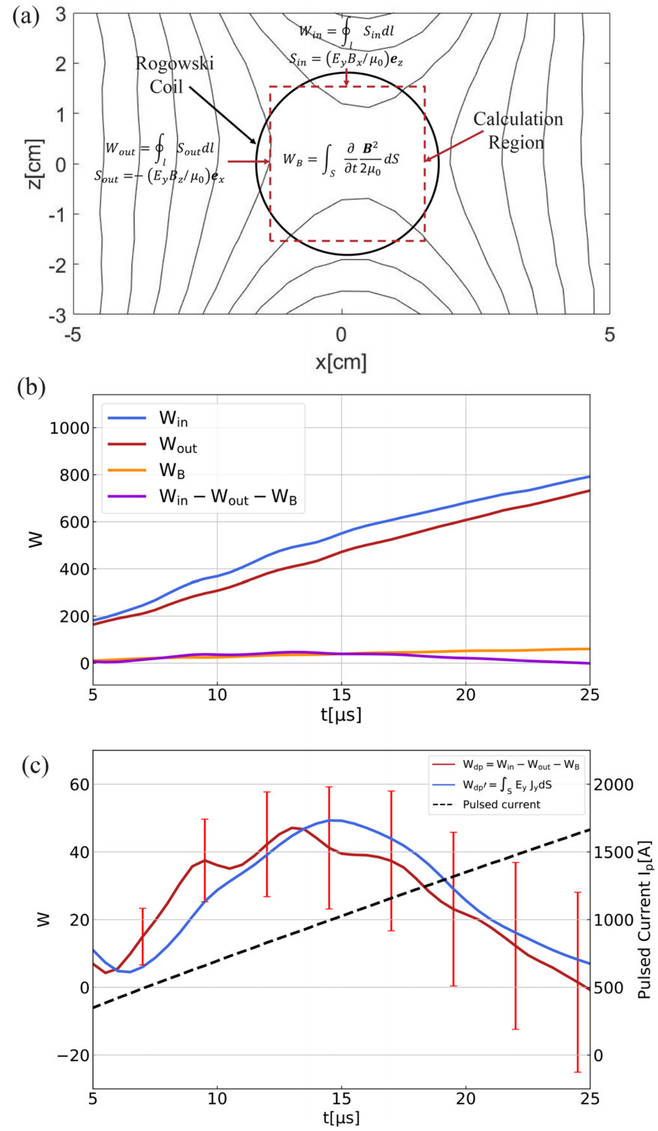

FIG. 5. (a) Schematic of the calculation of energy dissipation in the case at a ramp-up rate of 40 A/μs. The dashed quadrangle is the calculation region and the solid circle is the measurement region of the Rogowski coil. (b) Time evolution of the calculated terms of the Poynting theorem: W_{in}, W_{out}, and W_B. (c) Time evolution of energy dissipation calculated in two different ways and the pulsed current plotted as a dashed line for reference.

field obtained by the time integration of the magnetic probe will increase with the integration time, and it is used as the error bars of W_{dp}. The figure shows that the time evolution of W_{dp} and W'_{dp} are similar and satisfy Eq. (2). These two terms reach their peaks at approximately $t = 13$ and 14 μs, when the out-of-plane current also reaches its peak. It is found that about 10% of the incoming electromagnetic energy is transferred into plasma energy.

At the different ramp-up rates of the pulsed currents, the peak values of W_{dp} and W_{dp}/W_{in} when W_{dp} reaches its peak value are presented in Fig. 6. The peak values of W_{dp} increase almost linearly with

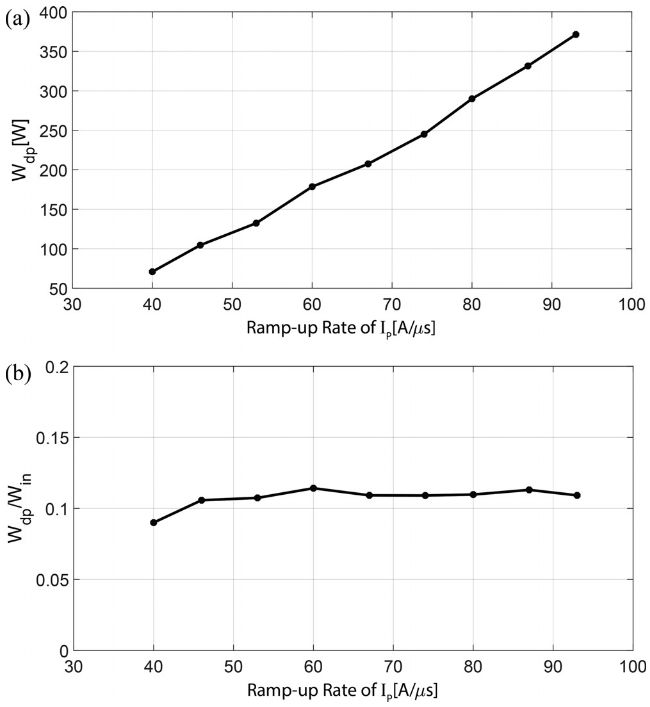

FIG. 6. (a) Peak values of W_{dp} in the denoted region at different ramp-up rates of the pulsed currents. (b) Corresponding value W_{dp}/W_{in} when W_{dp} reaches its peak value at different ramp-up rates of the pulsed currents.

the ramp-up rate of the pulsed currents, but W_{dp}/W_{in} hardly changes with an increase in the ramp-up rate. Therefore, we deduce that the percentage of energy conversion from the incoming electromagnetic to plasma energy remains almost constant even if the driving currents changes.

IV. CONCLUSIONS AND DISCUSSION

Experiments of electron-scale magnetic reconnection with a finite guide field have been conducted in our KLMP device, which are driven by two pulsed currents in two parallel 120-cm-long aluminum rods separated by 10 cm. With the progression of magnetic reconnection, we observe the enhancement of the out-of-plane current in the vicinity of the X line and the appearance of both plasma inflow and outflow. The inflow velocity is about 5000 m/s. We also measured the dissipation of magnetic energy in the vicinity of the X line and the conversion of incoming electromagnetic energy into plasma energy.

We further studied the effect of the ramp-up rate of the pulsed current on magnetic reconnection. With an increase in the ramp-up rate, both the inflow velocity and the conversion of incoming electromagnetic energy into plasma energy increase. However, the percentage of the incoming electromagnetic energy into plasma energy is about 10% and almost independent of the ramp-up rate.

Electron-scale reconnection has also been reported in other experiments and satellite observations.[26,30–32] Shi *et al.*[26] measured the energy dissipation in experimental electron-scale reconnection with a strong guide field ($B_g > 20B_r$) and found the ratio of electron enthalpy flux to Poynting flux reaches 70%, which is much higher than that in our experiments. We think that this higher ratio may come from the stronger guide field. When these exist, a strong guide field, the electrons are easier to be trapped in the X line region and continuously gain acceleration by the parallel electric field.[33,34] The observations from the MMS satellite[30–32] have also shown that in electron-scale reconnection, half of the incoming Poynting flux is converted into electron kinetic energy and the other half may appear as electron heating. In addition, previous simulation and experimental works have shown that the process of energy conversion can occur in other regions, e.g., the dipolarization fronts (DFs)[35,36] and the separatrix region.[26] This important issue of energy dissipation in electron-scale reconnection will be investigated in our future work when the diagnostic systems such as LIF and TS (measure the IVDF and EEDF) are fully developed.

ACKNOWLEDGMENTS

This work was supported by the Strategic Priority Research Program of Chinese Academy of Sciences; Grant No. XDB 41000000, the Key Research Program of Frontier Sciences, CAS (No. QYZDJ-SSW-DQC010), and Fundamental Research Funds for the Central Universities Grant Nos. WK3420000006 and WK2080000135.

AUTHOR DECLARATIONS

Conflict of Interest

The authors have no conflicts to disclose.

Author Contributions

Longlong Sang: Formal analysis (equal); Investigation (lead); Methodology (lead); Writing – original draft (lead); Writing – review & editing (equal). **Quanming Lu:** Conceptualization (equal); Formal analysis (equal); Funding acquisition (equal); Project administration (equal); Supervision (equal); Writing – review & editing (lead). **Jinlin Xie:** Data curation (equal); Formal analysis (equal); Methodology (equal); Writing – review & editing (lead). **Feibin Fan:** Investigation (equal); Writing – original draft (equal). **Qiaofeng Zhang:** Methodology (equal); Validation (equal). **Weixing Ding:** Supervision (equal); Validation (equal). **Jian Zheng:** Validation (equal). **Xuan Sun:** Validation (equal).

DATA AVAILABILITY

The data that support the findings of this study are available from the corresponding authors upon reasonable request.

REFERENCES

[1]V. M. Vasyliunas, Rev. Geophys. **13**, 303, https://doi.org/10.1029/RG013i001p00303 (1975).
[2]E. Priest and T. Forbes, *Magnetic Reconnection: MHD Theory and Applications* (Cambridge University Press, Cambridge, UK, 2000).
[3]R. G. Giovanelli, Nature **158**, 81–82 (1946).
[4]S. Tsuneta, Astrophys. J. **456**, 840 (1996).
[5]D. N. Baker, T. I. Pulkkinen, T. I. Angelopoulos, W. Baumjohann, and R. L. McPherron, J. Geophys. Res. **101**(A6), 12975–13010, https://doi.org/10.1029/95JA03753 (1996).
[6]R. Wang, Q. Lu, A. Du, and S. Wang, Phys. Rev. Lett. **104**, 175003 (2010).

[7]M. Hesse, K. Schindler, J. Birn, and M. Kuznetsova, Phys. Plasmas **6**(5), 1781–1795 (1999).
[8]H. J. Cai, D. Q. Ding, and L. C. Lee, J. Geophys. Res. **99**(A1), 35–42, https://doi.org/10.1029/93JA02519 (1994).
[9]M. Hesse, M. Kuznetsova, and M. Hoshino, Geophys. Res. Lett. **29**(12), 4-1–4-4, https://doi.org/10.1029/2001GL014714 (2002).
[10]J. Egedal, J. Ng, A. Le, W. Daughton, B. Wetherton, J. Dorelli, D. Gershman, and A. Rager, Phys. Rev. Lett. **123**(22), 225101 (2019).
[11]J. Birn, J. F. Drake, M. A. Shay, B. N. Rogers, R. E. Denton, M. Hesse, M. Kuznetsova, Z. Ma, A. Bhattacharjee, A. Otto, and P. L. Pritchett, J. Geophys. Res. **106**, 3715, https://doi.org/10.1029/1999JA900449 (2001).
[12]Y. Yi, M. Zhou, L. Song, and X. Deng, Astrophys. J. Lett. **883**(1), L22 (2019).
[13]M. Yamada, J. Yoo, J. Jara-Almonte, H. Ji, R. M. Kulsrud, and C. E. Myers, Nat. Commun. **5**(1), 5774 (2014).
[14]R. L. Stenzel and W. Gekelman, Phys. Rev. Lett. **42**, 1055–1057 (1979).
[15]R. L. Stenzel and W. Gekelman, J. Geophys. Res. **86**, 649, https://doi.org/10.1029/JA086iA02p00649 (1981).
[16]M. Yamada, Y. Ono, A. Hayakawa, M. Katsurai, and F. W. Perkins, Phys. Rev. Lett. **65**, 721–724 (1990).
[17]Y. Ono, M. Yamada, T. Akao, T. Tajima, and R. Matsumoto, Phys. Rev. Lett. **76**, 3328–3331 (1996).
[18]M. Yamada, H. T. Ji, S. Hsu, T. Carter, R. Kulsrud, Y. Ono, and F. Perkins, Phys. Rev. Lett. **78**, 3117–3120 (1997).
[19]H. T. Ji, M. Yamada, S. Hsu, and R. Kulsrud, Phys. Rev. Lett. **80**, 3256–3259 (1998).
[20]I. Furno, T. Intrator, E. Torbert, C. Carey, M. D. Cash, J. K. Campbell, W. J. Fienup, C. A. Werley, and G. A. Wurden, Rev. Sci. Instrum. **74**, 2324–2331 (2003).
[21]T. P. Intrator, X. Sun, G. Lapenta, L. Dorf, and I. Furno, Nat. Phys. **5**, 521–526 (2009).
[22]J. Olson, J. Egedal, S. Greess, R. Myers, M. Clark, D. Endrizzi, K. Flanagan, J. Milhone, E. Peterson, J. Wallace, D. Weisberg, and C. B. Forest, Phys. Rev. Lett. **116**, 255001 (2016).
[23]A. G. Frank and S. Y. Bogdanov, Earth Planets Space **53**, 531–537 (2001).
[24]A. V. Stechow, O. Grulke, and T. Klinger, Plasma Phys. Controlled Fusion **58**, 014016 (2015).
[25]N. Jain, A. V. Stechow, P. A. Muñoz, J. Büchner, O. Grulke, and T. Klinger, Phys. Plasmas **24**, 092312 (2017).
[26]P. Shi, P. Srivastav, M. H. Barbhuiya, P. A. Cassak, E. E. Scime, and M. Swisdak, Phys. Rev. Lett. **128**(2), 025002 (2022).
[27]F. Fan, J. Xie, Q. Zhang, L. Sang, and W. Ding, Chin. Phys. Lett. **36**(1), 015201 (2019).
[28]R. L. Stenzel, W. Gekelman, and N. Wild, J. Geophys. Res. **87**, 111, https://doi.org/10.1029/JA087iA01p00111 (1982).
[29]D. Wendel, D. K. Olson, M. Hesse, N. Aunai, M. Kuznetsova, H. Karim Ab Adi, W. Daughton, and M. L. Adrian, Phys. Plasmas **20**(12), 122105 (2013).
[30]T. D. Phan, J. P. Eastwood, M. A. Shay, J. F. Drake, B. U. Ö. Sonnerup, M. Fujimoto, P. A. Cassak, M. Øieroset, J. L. Burch, R. B. Torbert, A. C. Rager, J. C. Dorelli, D. J. Gershman, C. Pollock, P. S. Pyakurel, C. C. Haggerty, Y. Khotyaintsev, B. Lavraud, Y. Saito, M. Oka, R. E. Ergun, A. Retino, O. L. Contel, M. R. Argall, B. L. Giles, T. E. Moore, F. D. Wilder, R. J. Strangeway, C. T. Russell, P. A. Lindqvist, and W. Magnes, Nature **557**(7704), 202–206 (2018).
[31]R. Wang, Q. Lu, R. Nakamura, W. Baumjohann, C. Huang, C. T. Russell, J. L. Burch, C. J. Pollock, D. Gershman, R. E. Ergun, S. Wang, P. A. Lindqvist, and B. Giles, Geophys. Res. Lett. **45**(10), 4542–4549, https://doi.org/10.1002/2017GL076330 (2018).
[32]S. Lu, R. Wang, Q. L. V. Angelopoulos, R. Nakamura, A. V. Artemyev, P. L. Pritchett, T. Z. Liu, X. J. Zhang, W. Baumjohann, W. Gonzalez, A. C. Rager, R. B. Torbert, B. L. Giles, D. J. Gershman, C. T. Russell, R. J. Strangeway, Y. Qi, R. E. Ergun, P. A. Lindqvist, J. L. Burch, and S. Wang, Nat. Commun. **11**(1), 5049 (2020).
[33]X. Fu, Q. Lu, and S. Wang, Phys. Plasmas **13**, 012309 (2006).
[34]C. Huang, Q. Lu, and S. Wang, Phys. Plasmas **17**(7), 072306 (2010).
[35]K. Huang, Q. Lu, S. Lu, R. Wang, and S. Wang, J. Geophys. Res. **126**(10), e2021JA029939, https://doi.org/10.1029/2021JA029939 (2021).
[36]Y. Shu, S. Lu, Q. Lu, W. Ding, and S. Wang, J. Geophys. Res. **126**(10), e2021JA029712, https://doi.org/10.1029/2021JA029712 (2021).